

## **Design of wide area fractional-order PID damping controller for inter-area low-frequency oscillations using differential evolution**

Saleh M. Bamasak\*, Sreerama Kumar R. and Yusuf A. Al-Turki

*Department of Electrical & Computer Engineering, King Abdulaziz University, Jeddah 21589, Saudi Arabia*

*\* Saudi Electricity Company, Jeddah, Saudi Arabia*

*\* Corresponding Author: s.m.bamasak@ieee.org*

### **ABSTRACT**

A Wide Area Measurement System (WAMS) can extend and effectively improve a controllers' capability of damping inter-area low-frequency oscillations in interconnected power systems. This paper presents an implementation of a Wide Area Fractional-Order Proportional-Integral-Derivative (WA-FOPID) damping controller to improve the system damping. A modal analysis approach is proposed to identify the best location for the WA-FOPID controller and the optimal combination of input signals. The differential evolution optimization algorithm is used to determine the optimal controller parameters, and a nonlinear time-domain-based objective function is formulated to minimize the time-weighted errors. The proposed approach is successfully applied to a two-area four-machine system, as well as to a practical multi-area power system. The nonlinear time-domain simulations indicate that the proposed WA-FOPID damping controller can effectively dampen inter-area oscillations and improve system stability, irrespective of the severity or location of disturbances.

**Keywords:** Differential evolution (DE); fractional-order PID (FOPID); oscillation damping; phasor measurement unit (PMU); wide area damping controller (WADC).

#### Nomenclature

CPSS	: Conventional Power System Stabilizer
FOPID	: Fractional-Order Proportional-Integral-Derivative
PSO	: Particle Swarm Optimization
FACTS	: Flexible AC Transmission System
TCSC	: Thyristor-Controlled Series Compensation
AGC	: Automatic Gain Control
LFO	: Low-Frequency Oscillations
PSS	: Power System Stabilizer
PMU	: Phasor Measurement Unit
WAMS	: Wide Area Measurement System

$K_A, T_A$	: Gain and time constant of the excitation system
GPS	: Global Positioning System
$D$	: Damping coefficient, puMW/Hz
$M$	: Generator inertia constant
$T_m$	: Input torque of the generator, p.u.
$T_e$	: Output torque of the generator, p.u.
$E'_q, E_{fd}$	: Internal voltage of the machine, V
$i_d, i_q$	: d- and q-axis armature currents, A
$x_d, x'_d$	: d-axis reactance and d-axis transient reactance, $\Omega$
$\delta$	: Generator rotor angle, $^\circ$
$\omega_b$	: Base angular velocity, p.u.
$\omega$	: Angular velocity, p.u.

## INTRODUCTION

Nowadays, power system networks are becoming more complex, and an increasing number of tie-lines are linking adjacent areas and, in some cases, loading networks very close to their capacity limits. At the same time, the low-frequency oscillations that result from heavy loading conditions limit the utilization of tie-lines up to their full capacity.

For decades, the damping of inter-area oscillations has been accomplished by installing Power System Stabilizers (PSSs) (Sauer et al., 1998; Yu, 1983). Each installed PSS receives a local signal such as the generator speed or power, as the input, and provides a supplementary signal to the generator excitation control. Although these local-measurement-based PSSs can provide sufficient damping for local mode oscillations, they demonstrate limited effectiveness in damping inter-area mode oscillations (Aboul-Ela et al., 1996; Kamwa et al., 2001). To address this problem, many researchers have explored the effectiveness of wide area measurements in wide area damping controllers (WADCs) for damping inter-area oscillations.

The use of remote signals as inputs has been proved to enhance the dynamic performance of the power system and dampen inter-area oscillations (Zhang et al., 2008). Many different approaches have been proposed for the design of WADCs, such as the phase-shift compensation technique (Huang et al., 2004), fruit fly optimization (Liu et al., 2014), fuzzy control (Lin, 2013), artificial neural networks (Lokman et al., 2013), backtracking search algorithm (BSA) (Shafiullah et al., 2015), hybrid energy-based wide area function (Yousefian et al., 2017), and robust control (Wang et al., 2014). However, the controllers developed based on these techniques are integer controllers. Because many physical systems are realized using fractional-order differential equations, better performance can be ensured by implementing fractional-order controllers (Ahuja et al., 2014). A FOPID controller, as proposed in Podlubny (1999), can provide better performance than the conventional PID controllers; this is validated by analyzing the dynamic responses of the FOPID controllers.

In FOPID controllers, the derivative and integral operations are of fractional-order. Therefore, in addition to tuning the proportional ( $K_p$ ), derivative ( $K_d$ ), and integral ( $K_i$ ) gains, two more parameters are used—the powers of  $s$  in the derivative and integral actions,  $\mu$  and  $\lambda$ , respectively. These additional parameters add flexibility and make the system more robust than its integer counterpart, thereby enhancing the dynamic performance. The proposed controller is a five-dimensional hyperspace optimization, as it requires finding an optimal set of values for  $K_p$ ,  $K_d$ ,  $K_i$ ,  $\lambda$ , and  $\mu$  to meet the specifications for a given process plant (Zhao et al., 2009). Thus, the FOPID controller uses the following parameters: proportional gain, derivative gain, integral gain, derivative order, and integral order.

The application of FOPID controllers to improve the power system oscillations damping has been explored to some extent. In Zhao et al. (2009), the system responses to disturbances were compared to those observed when using conventional PID controllers. In Bamasak et al. (2014), Particle Swarm Optimization (PSO) was implemented to tune the FOPID oscillation damping controller for a Flexible AC Transmission System (FACTS) device in a single machine infinite bus (SMIB). More recently, FOPID was studied as a means of improving system stability in multimachine power systems (Morsali et al., 2015). FOPID was applied in Thyristor-Controlled Series Compensation- (TCSC-) based damping controllers in coordination with Automatic Gain Control (AGC) to improve the overall system stability (Morsali et al., 2017). The Bacterial Foraging Optimization Algorithm (BFOA) was proposed by Arya, Y. & Kumar, N. (2017) to tune the FOPID parameters and was tested on a three-multi-area power system. In all these papers, local feedback signals were used in the damping controller.

In this paper, a Differential Evolution (DE) algorithm is proposed for simultaneously tuning a WA-FOPID controller and a Conventional Power System Stabilizer (CPSS) for damping inter-area low-frequency oscillations. The optimal WADC location, input signals, and controller design are also addressed. Modal analysis is used to determine the optimal location and the proper remote input signals. A time-weighted integral error index is implemented to tune the proposed controller's parameters. The performance of the proposed controller is investigated for a two-area power system. Time-domain simulations are performed to evaluate the performance of the proposed controller, and the results are compared with those of conventional WADCs.

### Fractional-order PID (FOPID) overview

A FOPID controller is a generalization of the typical PID controller. The main idea is to introduce an operator  $D$ , associated with the orders  $\lambda$  and  $\mu$ , which are not limited to integers. The differential equation for the FOPID controller is described as

$$u(t) = K_p e(t) + K_i D_t^{-\lambda} e(t) + K_D D_t^\mu e(t) \quad (1)$$

The Laplace transform is used to obtain the continuous transfer function of the FOPID controller as follows:

$$G(s) = K_p + K_i s^{-\lambda} + K_D s^\mu \quad (2)$$

The design of a FOPID controller includes tuning the following parameters:  $K_p$ ,  $K_d$ ,  $K_i$ ,  $\lambda$ , and  $\mu$ , which can take noninteger values. The fractional-order controller improves the conventional

PID controller from points to plane. Fig. 1 shows a comparison of the control possibilities using a FOPID controller and the four control points of a classical PID controller (Vilanova & Visioli, 2012). Such extension offers more flexibility in realizing the control purposes.

For industrial simulations and implementations, the transfer functions involve fractional orders of  $s$ , and it is necessary to implement approximations for the usual (integer-order) transfer functions. To approximate a fractional function correctly, a usual transfer function should engage an infinite number of zeroes and poles. In this paper, the FOPID differential equation has been solved using MATLAB code, by implementing rational approximations as discussed in Tracaud & Chen (2010).

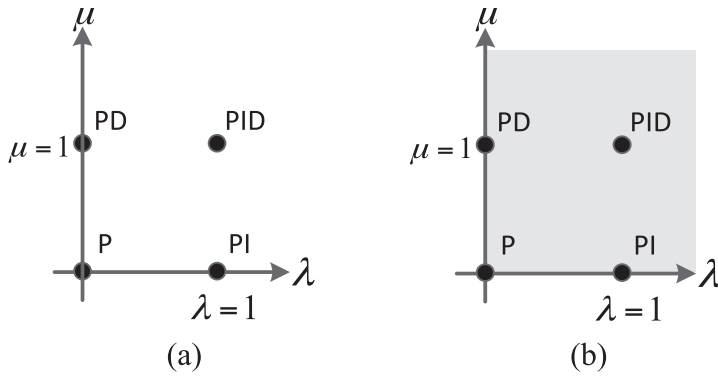


**Figure 1:** FOPID vs Classical PID: from point to plane: (a) integer-order controller and (b) fractional-order controller.

### POWER SYSTEM MODELING

A 2-area 4-machine power system is used in our study. The modeling of system components is described below.

#### Generator

A power system network consists of  $n$  generators; the third-order model is considered for each generator, which consists of swing equations and equations for the internal voltage  $E'_q$  of the generator, behind the transient reactance  $x'_d$ . The generators are assumed to have an excitation system consisting of PSSs (Yu, 1983). The equations of the  $i^{th}$  generator corresponding to this dynamic model are as follows:

$$\dot{\delta} = \omega_b(\omega - 1) \tag{3}$$

$$\dot{\omega} = (T_m - T_e - D(\omega - 1))/M \tag{4}$$

$$E'_q = (E_{fd} - (-x'_d + x_d) * i_d - E'_q)/(T'_{d0}) \tag{5}$$

#### Excitation system

The excitation system for the generators is assumed to be an IEEE Type ST1 system (Lee et al., 1992). The system transfer function is shown in Fig. 2. A damping controller attached to the excitation system uses the deviations in the generator angular velocity as input. In this study, the damping controller may be a (1) CPSS, (2) classic WADC, or (3) WA-FOPID controller.

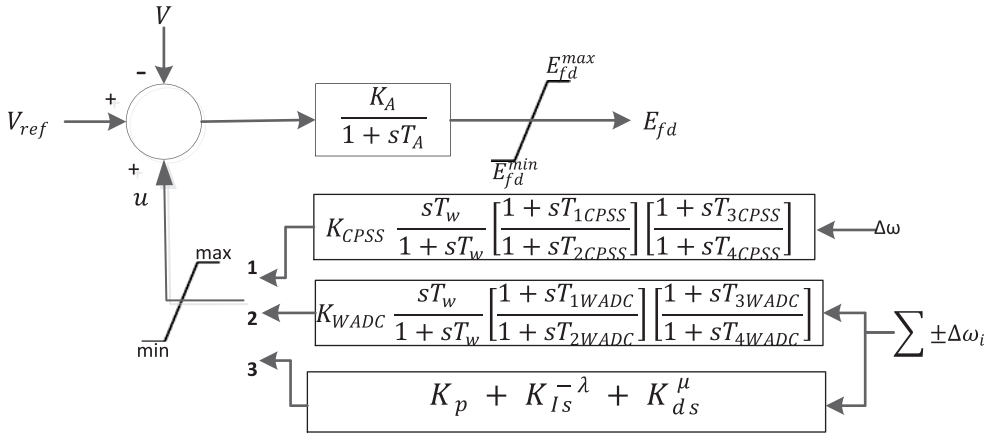


**Figure 2:** Excitation system model IEEE ST1 with damping controllers.

The IEEE ST1 model is represented by the equation

$$\dot{E}_{fd} = (K_A \times (-v + V_{ref} + U) - E_{fd}) / (T_A) \tag{6}$$

where  $K_A$  and  $T_A$  are the gain and time constant, respectively.

### Wide area FOPID

As shown in Fig. 3, in the proposed WA-FOPID damping controller, the stabilizing signals are measured by the Phasor Measurement Units (PMUs). These measured signals are time-synchronized using a Global Positioning System (GPS) and then transmitted to the controller. Then, the WA-FOPID controller generates the necessary control signals to prompt the generator excitation system to dampen the inter-area oscillations.

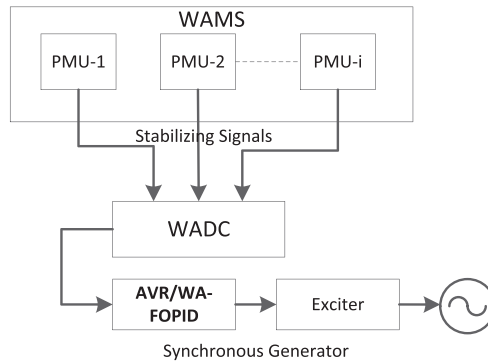


**Figure 3:** Structure of Wide Area Damping Control.

### Linearized multimachine system model

The power system dynamics are generally represented by a set of nonlinear differential equations (Kundur, 1994) given by

$$\dot{\mathbf{x}} = f(\mathbf{x}, \mathbf{U}) \quad (7)$$

where the variable of state vector is represented by  $\mathbf{x} = [\delta, \omega, E'_q, E'_{fd}]^T$ , and  $\mathbf{U}$  is the stabilizing input vector given by  $\mathbf{U} = [U \ ]^T$ . The design of the damping controllers utilizes a linearized incremental model around an operating point (Yu & Elsharkawi, 1981). Linearization of (07) yields the following:

$$\Delta \dot{\mathbf{x}} = \mathbf{A} \Delta \mathbf{x} + \mathbf{B} \mathbf{U} \quad (8)$$

$$\Delta \mathbf{y} = \mathbf{C} \Delta \mathbf{x} + \mathbf{D} \Delta \mathbf{u} \quad (9)$$

where

$\Delta \mathbf{x}$  represents the state vector increment for  $n$  machines;

$\Delta \mathbf{y}$  represents the output vector increment for  $m$  stabilizers;

$\Delta \mathbf{u}$  represents the  $r$  input vector increment;

$\mathbf{A}$  is a  $(4n \times 4n)$ ;

$\mathbf{B}$  is a  $(4n \times m)$ ;

$\Delta \mathbf{x}$  is a  $(4n \times 1)$ ;

$\mathbf{U}$  is an  $(m \times 1)$ .

## DESIGN OF WIDE AREA FOPID DAMPING CONTROLLER

A WA-FOPID controller utilizes remote measurements as feedback signals to improve the inter-area oscillation damping. To achieve an acceptable level of damping control, the location of the controller and the selection of the control inputs are critical. Two measurements are relevant in the design of the WA-FOPID controller (Dominguez-Garcia et al., 2014)—the observability measurement, which defines the observation machines based on their output signals, and the controllability measurement, which defines the control machines based on their input signals with respect to the interested mode of oscillation. Thus, when the output signal  $\Delta\omega$  of the  $j^{\text{th}}$  machine has the maximum mode observability, and the input signal  $\mathbf{u}_{pss}$  of the  $k^{\text{th}}$  machine has the maximum mode controllability with regard to the  $i^{\text{th}}$  inter-area mode, a preferable approach is to dampen the  $i^{\text{th}}$  mode by remotely feeding back the signal  $\Delta\omega$  of the  $j^{\text{th}}$  machine as an input to the WADC located at the  $k^{\text{th}}$  machine. Therefore, for the WA-FOPID controller, the controllability and observability measures can be derived from

$$Cont_{.ik} = |\Psi_i \mathbf{B}_k| \quad (10)$$

$$Obse_{.ji} = |\mathbf{C}_j \Phi_i| \quad , \quad (11)$$

where  $Cont_{.ik}$  is used to measure the controllability of the  $i^{\text{th}}$  mode from the  $k^{\text{th}}$  input and  $Obse_{.ji}$  measures the observability of the  $i^{\text{th}}$  mode from the  $j^{\text{th}}$  output.  $\Phi$  and  $\Psi$  are the right and left eigenvectors. To determine the best location for the CPSS and WA-FOPID controllers, the residue is considered as follows:

$$R_{jk}^i = C_k \Phi_i \Psi_i^T B_k \quad (12)$$

In the event that the output signal  $\Delta\omega_j$  has the highest observability, and the input signal  $U_{PSS}^k$  has the highest controllability concerning the  $i^{th}$  oscillation mode, it is suggested that the  $i^{th}$  mode be damped by feeding back as an input to the WA-FOPID controller located at the  $k^{th}$  machine.

### Differential Evolution- (DE-) based damping controller design and parameter tuning

DE is viewed as an evolutionary algorithm (Rainer et al., 1995) owing to its capacity to work in multimodal, nondifferentiable, and nonlinear objective functions. New offspring are created in DE, by forming a trial vector of each parent individual of a population. Selection, mutation, and crossover operations are performed to improve the effectiveness of the population in successive generations. The control parameters of the algorithm are the population size  $NP$ , the crossover constant  $CR$ , and the mutation constant  $F$ . The major stages in the DE algorithm are mentioned below.

#### i. Initialization

First, as preparation for the optimization process, the independent variables are initialized in their practical numerical ranges. If the lower and upper bounds of the  $j$ -th variable of a given problem are  $x_j^{max}$  and  $x_j^{min}$ , respectively, the  $j$ -th component of the  $i$ -th population member can be initialized as

$$x_{i,j} = x_j^{min} + rnd(0,1) * (x_j^{max} - x_j^{min}) \quad i = 1, NP; j = 1, D \quad (13)$$

Then, the objective value for each vector can be calculated using the initial population and can be compared to obtain the best solution. In each generation, this value is updated by comparison.

#### ii. Mutation

The mutation operation begins with the process of generating new solutions. In this stage, for every individual solution in the population in generation  $i$ :  $X_i^{(G)}$   $i = 1, \dots, NP$ , a mutant vector  $V_i^{(G+1)}$  is generated as

$$V_i^{(G+1)} = X_{r1}^{(G)} + F(X_{r2}^{(G)} - X_{r3}^{(G)}) \quad (14)$$

where  $X_{r2}^{(G)}$  and  $X_{r3}^{(G)}$  are solution vectors selected randomly from the current generation.  $X_{best}^{(G)}$  is the solution achieving the best value, and  $F$  is a mutation constant that has values in the range  $[1,0]$ . The factor  $F$  determines the speed of convergence.

#### iii Crossover

The crossover operation aims to improve the diversity of the generated solution. In this stage, the DE copies the generated mutant vector parameters, and its corresponding vector  $i$  in the original population, to a trial solution according to a crossover factor  $CR \in [1,0]$ . For each parameter, a comparison is carried out between a random number in the range  $[1,0]$  and the  $CR$ , and the parameter value is selected between the mutant vector and the parent as

$$u_{i,j}^G = \begin{cases} V_i^{(G)} & \text{if } rnd(0,1) < CR \\ x_{i,j} & \text{else} \end{cases} \quad (15)$$

where  $u_{i,j}^G$  represents the child that competes with the parent  $x_{i,j}$ .

#### iv. Selection

The last phase is to calculate the objective function for each trial vector and compare it with the solutions in the previous population. The one that gives the best result remains in the new population.

#### v. Stopping Criteria

Once a new generation is produced, the global best is updated. The stopping criterion chosen is the iterations maximum number.

### Tuning of parameters

An objective function  $J_{DE}$  is defined as an integral of time multiplied by the absolute error for speed deviation, for all machines.

$$J_{DE} = \int_0^3 t(\sum_1^n |\Delta\omega_i|) dt \quad (16)$$

The optimization problem of tuning the controller parameters is formulated as follows.

$$\text{Minimize } J \quad (17)$$

Subject to

$$K_{P\_min} \leq K_P \leq K_{P\_max}$$

$$K_{D\_min} \leq K_D \leq K_{D\_max}$$

$$K_{I\_min} \leq K_I \leq K_{I\_max}$$

$$\lambda_{min} \leq \lambda \leq \lambda_{max}$$

$$\mu_{min} \leq \mu \leq \mu_{max}$$

$$K_{min} \leq K_{PSS-i} \leq K_{max}$$

$$T_{1-PSS}^{min} \leq T_{1-PSS-i} \leq T_{1-PSS}^{max}$$

$$T_{3-PSS}^{min} \leq T_{3-PSS-i} \leq T_{3-PSS}^{max}$$

The limit range values of  $K_p$ ,  $K_I$ , and  $K_D$ , are set between 0.1 and 50. The  $\lambda$  and  $\mu$  parameters are in the range [0.001, 2]. The data for these ranges have been taken from Zamani et al. (2016).

Figure 4 shows a simplified schematic diagram of the interactions between DE and the dynamic simulations.

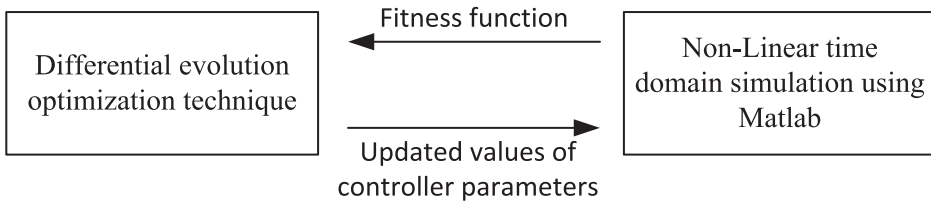


**Figure 4:** Integration of DE with nonlinear time-domain simulation

### SIMULATION RESULTS AND DISCUSSION

The effectiveness of the proposed controller in a multimachine power system network was evaluated using MATLAB-based simulations, for a two-area four-machine system. The simulation results for WA-FOPID controller were compared with those of the classic WADC and CPSS. The time constant for the reset block,  $T_w$ , was set to 10 s. Table 1 presents the values of the DE parameters.

**Table 1:** DE parameters.

DE control parameters	
Population size (NP)	50
Max. no. of gen. (GMAX)	100
Mutation (fm)	0.2
Crossover (CR)	0.6

#### Case Study 1: Two-area four-machine system

The two-area four-machine power network presented in Fig. 5 has two identical areas (Kundur, 1994), each with two 900 MVA generators. All four generators are represented by the third-order model. It is assumed that 400 MW power is transferred over the tie-line from the first area (Area 1) to the second (Area 2). The system data and initial conditions are presented in the appendix.

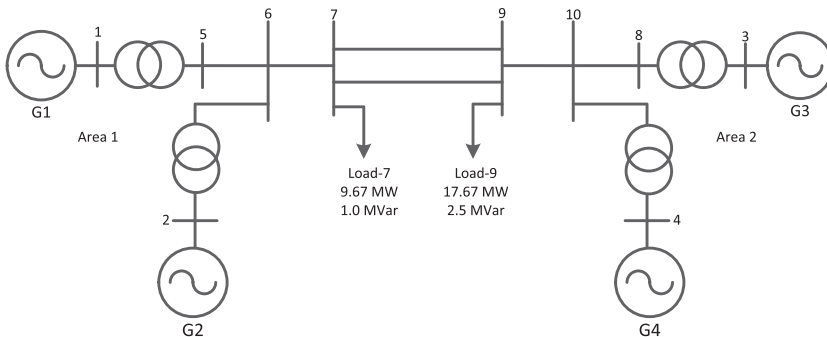


**Figure 5:** System single-line diagram.

Table 2 shows the system open-loop eigenvalues and their characteristics. From this table, it can be observed that three electromechanical modes are present in this system. These are (i) an inter-area mode, which has a negative damping ratio and a frequency of 0.6129 Hz, where the two generators that operate in Area 1 oscillate against Area 2 generators; (ii) a local mode, which has a frequency of 1.106 Hz, in which machines in Area 1 oscillate against each other; and (iii) a local mode, which has a frequency of 1.0741 Hz, where the machines in the Area 2 oscillate against each other.

**Table 2:** Open-Loop System Eigenvalues.

	<b>Eigenvalues</b>	<b>Frequency (Hz)</b>	<b>Damping Ratio</b>	<b>Mode of oscillations</b>
Mode 1	-1.2753 ± 6.949i	1.1060	0.1805	Local
Mode 2	-1.1983 ± 6.748i	1.0741	0.1748	Local
Mode 3	0.0281 ± 3.810i	0.6129	-0.0073	Inter-Area

The participation factors (PFs) for each machine in these three modes are shown in Table 3. Since the generators in each area are electrically close to each other, and all of them are identical, they have close values of PF for each mode of oscillation. For the inter-area mode, the table shows that Area 2 generators at the receiving end have higher PFs than Area 1 generators at the sending end.

**Table 3:** Machines’ Participation Factors in Oscillation Modes.

<b>Eigenvalues</b>	<b>Machines Participation Factor</b>			
	<b>Area 1</b>		<b>Area 2</b>	
	G1	G2	G3	G4
-1.2753 ± i6.9492	0.2867	0.3146	0.0052	0.0127
-1.1983 ± i6.7486	0.0110	0.0062	0.2890	0.3103
0.0281 ± i3.81	0.1200	0.0808	0.1631	0.1435

Once the dominant machine PFs are identified for each mode, the mode shapes can be determined from the magnitude and sign of the real part of the elements in the right eigenvector, related to the state variables involved in the mode. The rotor-angle right eigenvector elements for the three modes are shown in Table 4. For mode 1,  $G_1$  has a positive real part, whereas  $G_2$  has a negative real part. This indicates that  $G_1$  rotates against  $G_2$  locally, in Area 1. Similarly, the second local oscillation in Area 2 is between  $G_3$  and  $G_4$ , as these have different real part signs. Further, it can be inferred that mode 3 is an inter-area mode, since both  $G_1$  and  $G_2$  have the same sign for the real part, which is opposite to that of  $G_3$  and  $G_4$ . With this knowledge about the oscillatory modes, dominant machines, and their state variable participations in each mode, the local PSSs and WA-FOPID controllers can be designed. This design is discussed in the next section.

**Table 4:** Right-Eigenvector Elements (Corresponding to  $\Delta\delta$ ).

Mode 1	
Generator	Right Eigenvector Entry
1	0.0148 - 0.0472i
2	-0.01895 + 0.0458i
Mode 2	
Generator	Right Eigenvector Entry
3	0.0089 - 0.0488i
4	-0.0144 + 0.0480i
Mode 3	
Generator	Right Eigenvector Entry
1	-0.0240 + 0.0790i
2	-0.0286 + 0.0486i
3	0.0584 - 0.0948i
4	0.0491 - 0.0883i

*Optimal placement of the proposed controller*

From Table 3, it can be seen that  $G_2$  has the largest PF among all generators in oscillation mode 7. Thus, this machine has a greater effect on the oscillations in this mode than any other machine in the same area. Similarly, in mode 8,  $G_4$  has the largest PF. Thus, the local PSSs are located at  $G_2$  and  $G_4$ , in order to make the damping of the local-mode oscillations in these areas more effective. Further, as  $G_3$  has a higher participating inter-area oscillation than  $G_1$ , the WA-FOPID controller is located at  $G_3$ . A connectivity diagram of the proposed controller is shown in Fig. 6.

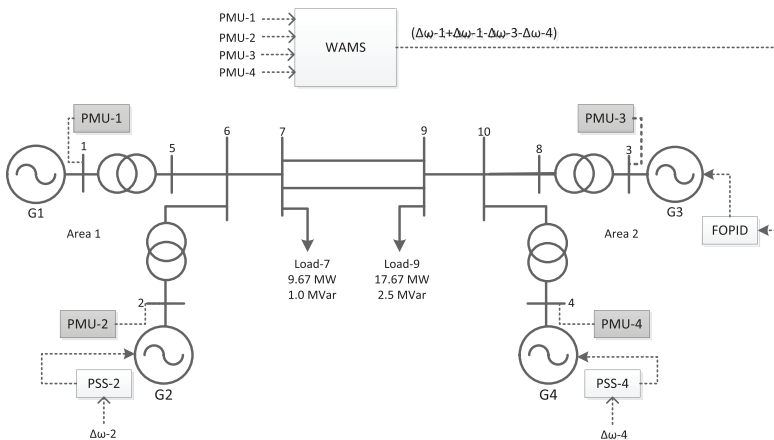


**Figure 6:** Connectivity diagram of the proposed controller for Two-Area Network.

To confirm the placement of the proposed controllers, measurements of controllability, observability, and residue should be obtained for all modes, as per equations (10)–(12). The overall damping stabilizer design enhances the damping in all oscillation modes. The residues of

the system generators correspond to the local modes of oscillation. Findings from modes 1 and 2 indicate that  $G_2$  has the largest magnitude in mode 1, and  $G_4$  has the largest magnitude in mode 2. Therefore, the CPSSs should be placed at  $G_2$  and  $G_4$ , which are the optimal locations for damping local-area oscillations. The inter-area mode controllability measurement is also used to confirm the placement of the WA-FOPID controller at  $G_3$ , since it has the largest controllability value. The feedback combination signal is  $(\sum_{k=1,2} \omega_k - \sum_{k=3,4} \omega_k)$ .

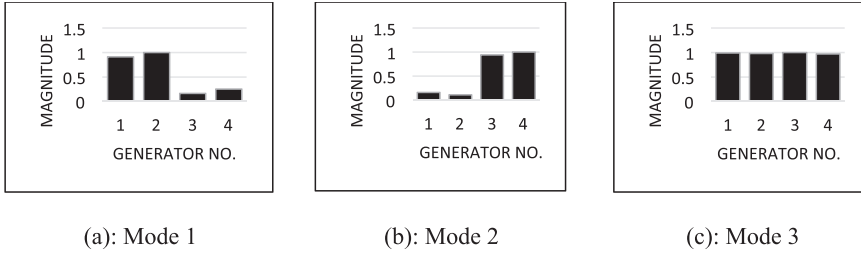


Figure 7: Controllability measures for all modes.

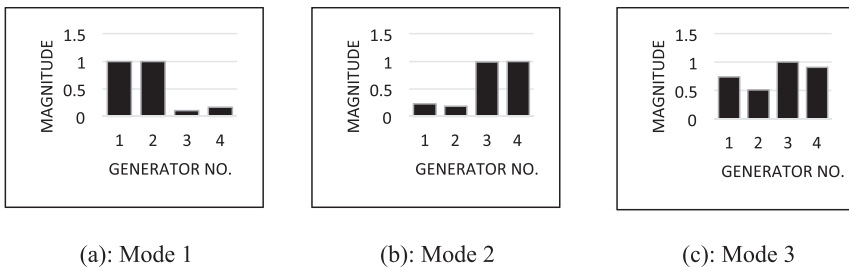


Figure 8: Observability measures for all modes.

Wide area FOPID and WADC parameter tuning using DE

Table 5 shows the optimal values for the controller parameters, obtained through the implementation of the DE algorithm for both the WA-FOPID controller and the WADC. The variations in the objective functions of the classic WADC and the WA-FOPID controller designs, with reference to the number of generations of the DE, are shown in Fig. 9.

Table 5: Optimal Settings of the Proposed Controller.

WA-FOPID @ machine-3		CPSS @ machine-2 & 4		
Parameters	Value	Parameters	PSS-2	PSS-4
$K_p$	29.558	K	88.176	14.3065
$K_D$	16.680	$T_1(s)$	0.0702	0.3246
$K_I$	06.180	$T_2(s)$	0.0500	0.0500
$\lambda$	1.3803	$T_3(s)$	0.0616	0.0021
$\mu$	0.916	$T_4(s)$	0.0500	0.0500

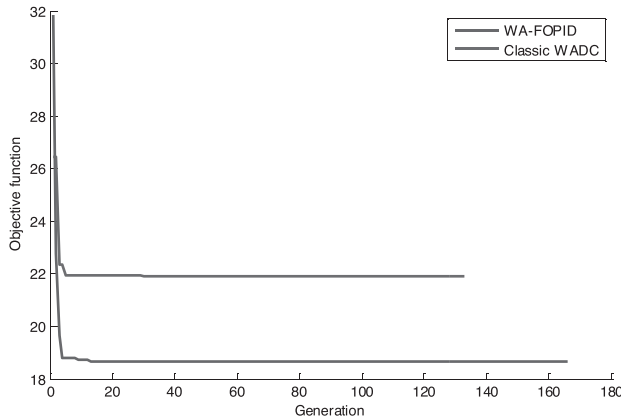


**Figure 9:** Variation of objective functions for DE-based optimization technique.

*Nonlinear time-domain simulation*

To validate the performance of the system with the proposed controllers, nonlinear time-domain simulations were carried out for a 3-ph fault of duration six cycles of 60 Hz at Bus#9. The simulations were conducted with different controllers: (i) three CPSSs, (ii) the classic WADC, and (iii) the proposed WA-FOPID controller. Fig. 10 and Fig. 11 show the variations in the rotor angles and the angular velocities of the machines in the system, corresponding to this disturbance. As seen in these figures, the system without the provision of any control experiences significant power oscillations. Further, it can be seen that the classic WADC dampens the inter-area oscillations better than the CPSS. The figures also indicate that the damping provided by the proposed WA-FOPID controller, along with the local CPSSs, is better than that provided by the classic WADC. The system with the WA-FOPID controller demonstrates the shortest settling time, zero steady-state error, and thus, an enhanced overall dynamic stability.

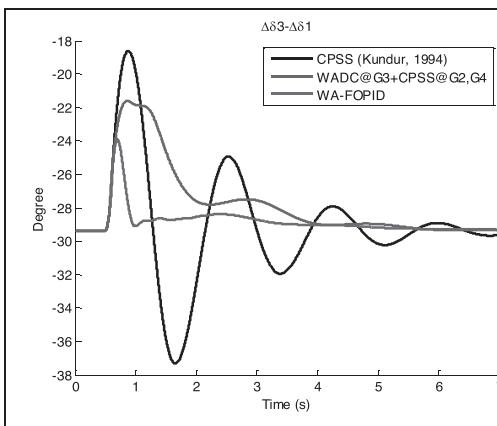


**Figure 10:** G3 relative angle responses for 3-ph short circuit.

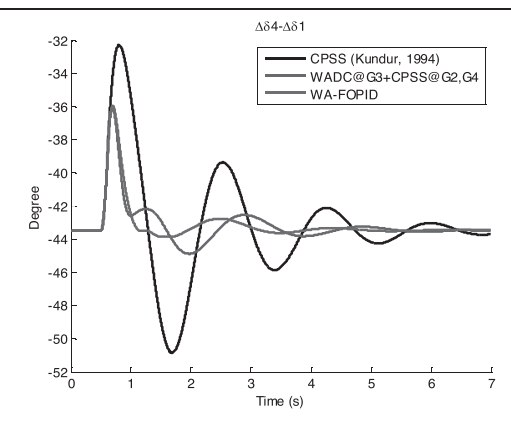


**Figure 11:** G4 relative angle responses for 3-ph short circuit.

Table 6 shows the settling time, peak, and mean sum squared error (MSSE) of the relative angle responses for the three controllers. It can be seen that the WA-FOPID controller achieves the least MSSE and that it minimizes the peak overshoot and settling time.

**Table 6:** Evaluation of Relative Angle Responses.

	G3 Relative angle responses			G4 Relative angle responses		
	$T_s$ (sec)	Overshoot %	MSSE	$T_s$ (s)	Overshoot %	MSSE
CPSS	>7	32.06	7.181e-4	>7	26.436 %	6.253e-4
WADC	5.7	24.13	5.679e-4	5.4	17.24 %	2.667e-4
WA-FOPID	4.5	17.01	2.071e-4	5.0	17.24 %	2.457e-4

**Case Study 2: Saudi electrical network**

The Saudi power grid 380 kV map and tie-lines diagram are shown in Fig. 12 and Fig. 13, respectively. Saudi power grid has four interconnected operating areas. In this paper, a reduced version of the Saudi 380 kV network is considered, which consists of 29 generators, 127 buses, and 222 circuits. The system reduction methodology has been presented in Al-Hajji et al. (2014), and it has been concluded that the reduced model is accurate and reliable for representing the dynamic characteristics of the complete system.



**Figure 12:** Saudi Arabia 380 kV Map.

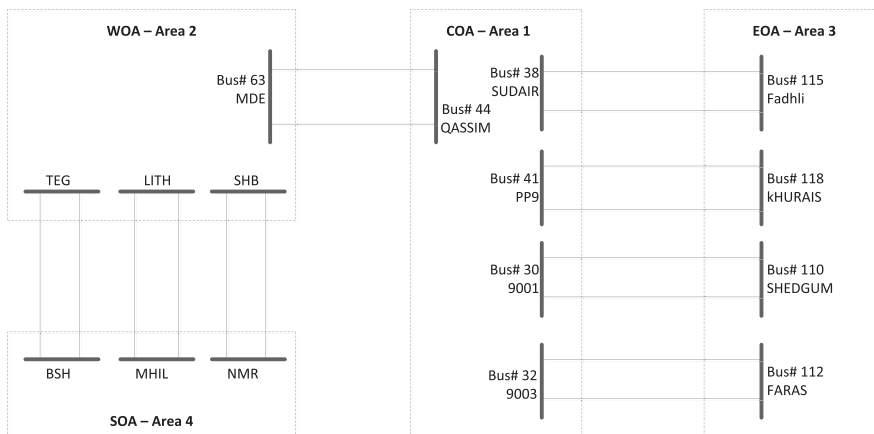


**Figure 13:** Saudi 380 kV Interconnection Tie-Lines.

The open-loop system eigenvalues are given in Table 7; they indicate that the system exhibits 28 electromechanical oscillation modes. All modes are classified as local modes except mode 28, which is classified as an inter-area mode of oscillation with an eigenvalue of  $-0.10402.449\pm i$ , frequency of 0.389 Hz, and a very low damping ratio of 0.042. The PF analysis has shown that Machine #28, which is located in Area 2, has the largest contribution to the inter-area mode.

Once the dominant machine PFs are identified for the inter-area mode, the mode shape can be determined from the elements in the right eigenvector related to the state variables involved in the mode. From the magnitude and sign of the real part of the eigenvector entries, the mode shape corresponding to the rotor angle states for mode 28 can be obtained; this is shown in Fig. 14. It indicates inter-area oscillations between Area 2 generators and the generators in Areas 1 and 3. More specifically, Generator 28 in Area 2 oscillates against units 16 and 11 in Area 3.

**Table 7: Open Loop System Analysis for Saudi Network.**

	<b>Eigenvalues</b>	<b>Freq. (Hz.)</b>	<b>Damping Ratio</b>
1	-0.4608 + 12.1695i	1.9368	0.037
2	-0.8865 + 11.0973i	1.7662	0.079
3	-0.2952 + 10.5184i	1.6740	0.028
4	-0.4867 + 10.5859i	1.6848	0.045
5	-0.4422 + 9.9178i	1.5784	0.044
6	-0.1872 + 9.4819i	1.509	0.019
7	-0.4349 + 9.3251i	1.4841	0.046
8	-0.3611 + 9.3704i	1.4913	0.038
9	-0.3552 + 8.8637i	1.4107	0.040
10	-0.3112 + 8.7874i	1.3985	0.035
11	-0.4485 + 8.2598i	1.3145	0.054
12	-0.2939 + 8.3084i	1.3223	0.035
13	-0.2897 + 8.2699i	1.3161	0.035
14	-0.2391 + 8.0673i	1.2839	0.029
15	-0.2200 + 7.6753i	1.2215	0.028
16	-0.2794 + 7.6203i	1.2128	0.036
17	-0.2734 + 5.4143i	0.86171	0.050
18	-0.4605 + 6.1002i	0.9708	0.075
19	-0.3709 + 7.5064i	1.19469	0.049
20	-0.2666 + 6.4366i	1.02442	0.041
21	-0.3372 + 7.0021i	1.11441	0.048
22	-0.3425 + 7.1568i	1.1390	0.047
23	-0.4280 + 7.2257i	1.1500	0.059
24	-0.4585 + 7.1232i	1.1336	0.064
25	-0.3088 + 6.5138i	1.0367	0.047
26	-0.2269 + 4.6636i	0.7422	0.048
27	-0.2444 + 4.8919i	0.7785	0.049
28	-0.1040 + 2.4490i	0.3897	0.042

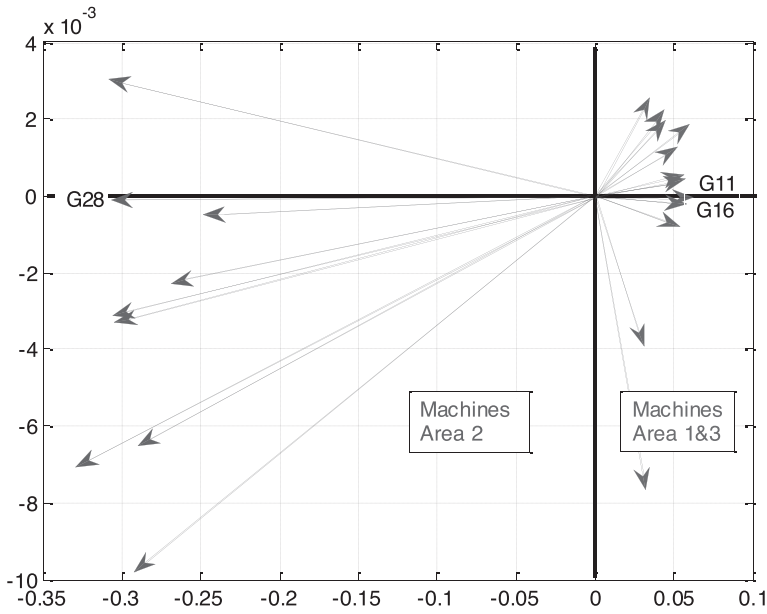


Figure 14: Mode shape for rotor angle (inter-area mode).

*Placement and design of the proposed controller*

The modal analysis has indicated that Generator 28 is the most dominant unit for the inter-area mode of oscillations. Hence, the proposed WA-FOPID damping controller will be placed at Unit 28 and the feedback combination signal will be  $(\sum_{k=28} \omega_k - \sum_{k=11,16} \omega_k)$ . The controller schematic structure is presented in Fig. 15. Comparing the damping ratio analyses, with and without the WA-FOPID controller, it can be observed that, without the WA-FOPID controller, the highest damping ratio of the rotor speed deviation is 0.079, whereas, after deploying the proposed controller, the highest damping ratio is 0.194. In general, by comparing the performances of the power systems without and with the WA-FOPID controller, it can be observed that the eigenvalues and their respective damping ratios show great improvements. Thus, it is quite clear that the overall dynamic performance is enhanced significantly after the deployment of the proposed controller.

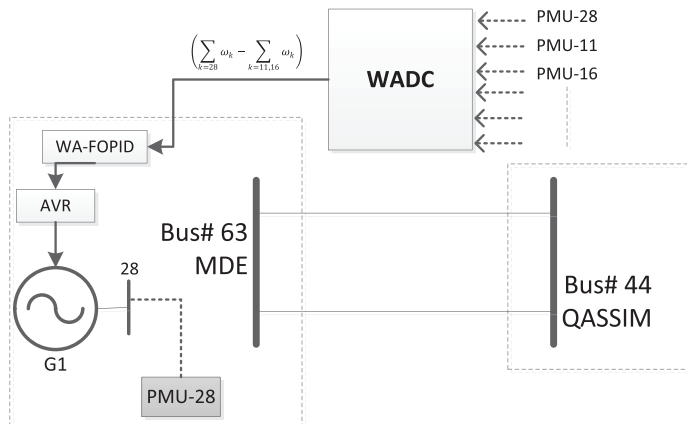
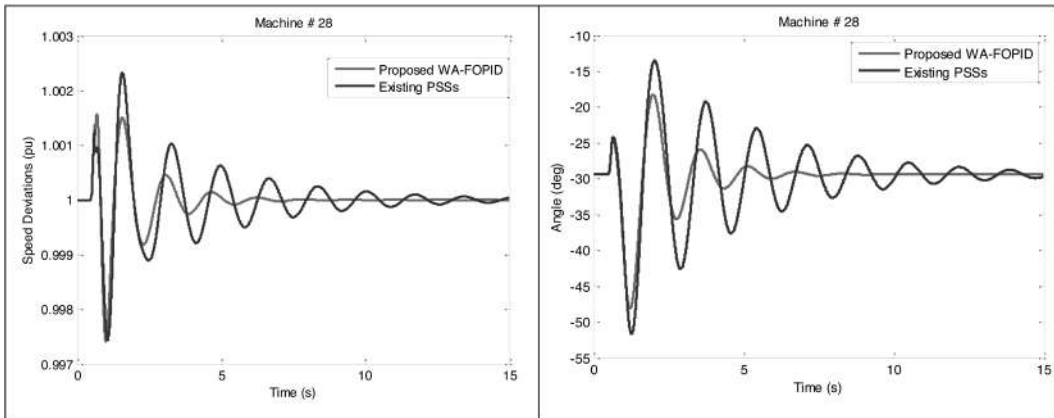


Figure 15: WA-FOPID Damping Controller Structure.

*Nonlinear time-domain simulation*

Fig. 10 and Fig. 17 show the speed deviation and rotor angle responses for a 3-ph short circuit. These figures compare the system dynamic stability before and after the deployment of the proposed WA-FOPID damping controller. By analyzing these figures, it is quite clear that the dynamic performances of the system with the proposed PSS show considerable improvement. For example, the settling times of Machine 28 in Area 2 are noticeably decreased by more than 15, to approximately 7 s.



**Figure 16:** G28 speed deviation response for 3-ph short circuit.

**Figure 17:** G28 angle response for 3-ph short circuit.

The existing maximum power transfer between COA and WOA is approximately 420 MW, after which the system goes out of synchronism and oscillates continuously. However, it can also be observed that, after deploying the optimized WA-FOPID controller, the dynamic stability of the system is improved considerably. Thus, the power transfer between the two areas can be increased far beyond the existing transfer level. To determine the maximum power transfer using the proposed controller, the same incident is repeated in this section. Fig. 18 shows that the maximum power is substantially increased, from 420 to 700 MW.

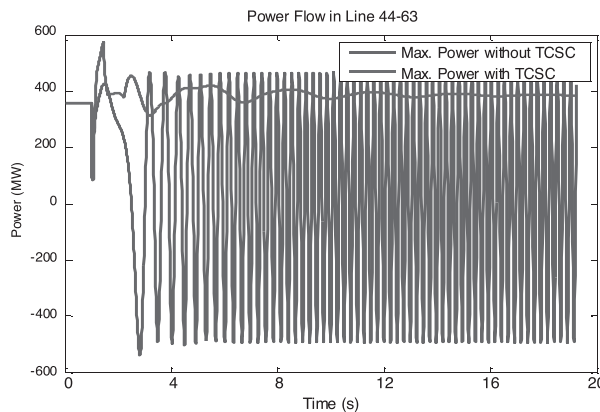


**Figure 18:** Power flow in COA-WOA tie-lines at (700 MW) power transfer.

### CONCLUSION

This paper reported an investigation into the effectiveness of a WA-FOPID system to enhance the power system stability. The controller-stabilizing signals were derived from the data acquired through the PMUs installed at different locations in the system. The WA-FOPID controller was designed such that it focused on stabilizing the inter-area oscillations in the system, while leaving the local modes of oscillation to be controlled by the local PSSs. The preliminary investigations indicated that the WA-FOPID damping controller showed a significantly better performance than the conventional integer controllers, even under severe disturbance conditions.

### ACKNOWLEDGMENT

The authors would like to acknowledge the support of the Saudi Electricity Company and King Abdulaziz University.

### APPENDIX

The two-area system data, load flow results, and initial conditions are given below.

**Table 8:** Generator and Exciter Data.

Gen.	$H$ (MW.s/MVA)	$X_d$ (pu)	$X_q$ (pu)	$X'_d$ (pu)	$X'_q$ (pu)	$T'_{do}$ (s)	$T'_{qo}$ (s)	$D$	$K_A$	$TA$ (s)
1	55.575	0.2	0.19	0.033	0.061	8	0.4	0	200	0.01
2	55.575	0.2	0.19	0.033	0.061	8	0.4	0	200	0.01
3	58.5	0.2	0.19	0.033	0.061	8	0.4	0	200	0.01
4	58.5	0.2	0.19	0.033	0.061	8	0.4	0	200	0.01

**Table 9:** System Bus Data.

Bus no.	Type	Voltage (pu)	Angle	Generation		Load	
				P (MW)	Q (MVAR)	P (MW)	Q (MVAR)
1	1	1.03	0			0	0
2	2	1.01		700		0	0
3	2	1.03		719		0	0
4	2	1.01		700		0	0
5	3	1.00		0	0	0	0
6	3	1.00		0	0	0	0
7	3	1.00		0	0	967	100
8	3	1.00		0	0	1767	250
9	3	1.00		0	0	0	0
10	3	1.00		0	0	0	0

Bus types: (1) Slack Bus, (2) PV Bus, (3) BQ Bus

**Table 10:** System Transmission Lines Data.

Line no.	From	To	R (p.u)	X (p.u)	B (p.u)
1	1	5	0	0.0576	0.00
2	2	6	0	0.0625	0.00
3	3	10	0	0.0586	0.00
4	4	9	0	0.0850	0.088
5	5	6	0.0025	0.025	0.021875
6	6	7	0.001	0.01	0.00875
7	7	8	0.011	0.11	0.385
8	8	9	0.001	0.01	0.00875
9	9	10	0.0025	0.025	0.021875

**Table 11:** System Load Flow Results.

Bus no.	Voltage (pu)	Angle (Degree)	Generation		Load	
			P (MW)	Q (MVAR)	P (MW)	Q (MVAR)
1	1.03	0	704.94	201.63	0	0
2	1.01	-9.9268	700.00	271.41	0	0
3	1.03	-28.7102	719.00	235.61	0	0
4	1.01	-39.0715	700.00	344.85	0	0
5	1.0038	-6.5378	0	0	0	0
6	0.9720	-16.7654	0	0	0	0
7	0.9504	-25.3242	0	0	967	100
8	0.9294	-54.8907	0	0	1767	250
9	0.9600	-45.9963	0	0	0	0
10	0.9986	-35.4139	0	0	0	0

**Table 12:** Machines Initial Conditions.

	$I_{di}$	$I_{qi}$	$V_{do}$	$V_{qo}$	$E_{fdo}$	$E_d'$
G <sub>1</sub>	6.089528	3.686605	0.700455	0.755157	1.973063	0.578797
G <sub>2</sub>	6.568511	3.479973	0.661195	0.763493	2.077195	0.546356
G <sub>3</sub>	6.381238	3.638824	0.691377	0.763478	2.039725	0.571295
G <sub>4</sub>	6.983409	3.305191	0.627986	0.791033	2.187715	0.518915

## REFERENCES

- Aboul-Ela, M., Sallam, A., McCalley, J. & Fouad, A. 1996.** Damping controller design for power system oscillations using global signals. *IEEE Trans. Power Syst.*, 11, Pp. 767–773.
- Ahuja, A. & Aggarwal, S. K. 2014.** Design of fractional order PID controller for DC motor using evolutionary optimization techniques. *Wseas Transactions on Systems And Control*, 9, Pp. 171–182.
- Al-Hajji, M. & Abido, M. 2014** "Systematic Approach for Dynamic Equivalents Development of Large-Scale Power System Using PSS/E ," GCC CIGRE, 10th International Conference, Bahrain.
- Arya, Y. & Kumar, N. 2017.** BFOA-scaled fractional order fuzzy PID controller applied to AGC of multi-area multi-source electric power generating systems. *Swarm and Evolutionary Computation*, 32, pp.202–218.
- Bamasak, S. M. & Bensenouci, A. 2014.** Tuning of fractional order PID controller for TCSC-based stabilizer using PSO for power system oscillation damping. *IEEE International Energy Conference*, Pp. 262–266.
- deMello, F. & Concordia, C. 1969.** Concepts of Synchronous Machine Stability as Affected by Excitation Control. *IEEE Trans.*, 88, Pp. 316–329.
- Domínguez-García, J. L., Ugalde-Loo, C. E., Bianchi, F. & Gomis-Bellmunt, O. 2014.** Input–output signal selection for damping of power system oscillations using wind power plants. *International Journal of Electrical Power & Energy Systems*, 58, 75–84.
- Huang, Y. & Xu , Z. 2004.** HVDC supplementary controller based on synchronized phasor measurement units. *Power Systems Conference and Exposition* Pp. 668–672.
- Kamwa, I., Grondin, R. & Hébert, Y. 2001.** Wide-area measurement based stabilizing control of large power systems-a decentralized/hierarchical approach. *IEEE Transactions on Power Systems*, 16(1), Pp. 136–153.
- Kundur, P. 1994.** *Power system stability and control.* (Vol. 7). (a. M. Eds. Neal J. Balu, Ed.) New York: McGraw-hill.
- Lee, D. C., Baker, D. H. & Bess, K. C. 1992.** IEEE Recommended practice for excitation system models for power system stability studies. Energy development and power generation committee of power engineering society.
- Lin, Y.J. 2013.** Proportional plus derivative output feedback based fuzzy logic power system stabiliser. *International Journal of Electrical Power & Energy Systems*, 44(1), Pp. 301–307.
- Liu, Y., Zhijian , H., Jianglei , S. & Ji , D. 2014.** Design method of wide-area damping controller based on FOA algorithm. *Intelligent Control and Automation (WCICA)* Pp. 4893–4897.
- Lokman, H. H., Moghavvemi, M. & Almurib, H. A. 2013.** Current state of neural networks applications in power system monitoring and control. *International Journal of Electrical Power & Energy Systems*, 51, Pp. 134–144.
- Ma, J., Wang, T., Yan, W. & Wang, Z. 2014.** Design of wide-area robust damping controller based on the non-convex stable region for inter-area oscillations. *International Journal of Electrical Power & Energy Systems*, 55, Pp. 473–480.
- Morsali, J., Kazemzadeh , R. & Azizian, M. R. 2015.** Introducing FOPID-PSS to increase small-signal stability of multi-machine power system. *IEEE 23rd Iranian Conference on Electrical Engineering*, Pp. 1510–1515.

- Morsali, J., Zare, K. & Hagh, M.T. 2017.** Applying fractional order PID to design TCSC-based damping controller in coordination with automatic generation control of interconnected multi-source power system. *Engineering Science and Technology, an International Journal*, 20(1), pp.1–17.
- Podludny, I. 1999.** Fractional-order systems and controllers. *IEEE Transactions on Automatic Control*, 44, 208–214.
- Rainer, S. & Price, K. 1995.** *Differential evolution-a simple and efficient adaptive scheme for global optimization over continuous spaces* (Vol. 3). Berkeley: ICSI.
- Sauer, P. W. & Pai, M. A. 1998.** *Power system Dynamics and Stability*. Prentice Hall.
- Shafiuallah, M., Abido, M. A. & Coelho, L. S. 2015.** Design of Robust PSS in Multimachine Power Systems using Backtracking Search Algorithm. *18th International Conference on Intelligent System Application to Power System*, Pp. 1–6. Portugal.
- TRICAUD C. & Y.Q. CHEN. 2010.** An approximation method for numerically solving fractional order optimal control problems of general form. *Computers & Mathematics with Applications*, 59, pp. 1644–1655.
- Vilanova, R. & Visioli, A. 2012.** *PID Control in the Third Millennium: Lessons Learned and New Approaches*. Springer.
- Xiao, F., Sun, Y., Yang, F. & Cheng, L. 2007.** Inter-area damping controller design based on mode controllability and observability. *International Power Engineering Conference, IPEC*, Pp. 95–99.
- Yousefian, R., Sahami, A. & Kamalasadani, S. 2017.** Hybrid Transient Energy Function-Based Real-Time Optimal Wide-Area Damping Controller. *IEEE Transactions on Industry Applications*, 53(2), pp.1506–1516.
- Yu, Y. N. 1983.** *Electric power system dynamics*. NEW YORK, USA: ACADEMIC PRESS.
- Yu Y. & El-Sharkawi M. 1981.** Estimation of External Dynamic Equivalents of a Thirteen-Machine System,” *IEEE Transactions on Power Apparatus and Systems*, vol. PAS-100, Mar. 1981, pp. 1324–1332.
- Yuan, Y., Sun, Y. & Cheng, L. 2008.** Determination of wide-area PSS locations and feedback signals using improved residue matrices. *IEEE Asia Pacific Conference on Circuits and Systems APCCAS*, Pp. 762–765.
- Zamani, A., Barakati, S.M. & Yousofi-Darmian, S. 2016.** Design of a fractional order PID controller using GBMO algorithm for load–frequency control with governor saturation consideration. *ISA transactions*, 64, pp.56–66.
- Zhang, Y. & Bose, A. 2008.** Design of Wide-Area Damping Controllers for Interarea Oscillations. *IEEE Trans. on Power Systems*, 23(3), Pp. 231–245.
- Zhao, Y., Gao, Y., Hu, Z., Zhan, J. & Zhang, Y. 2009.** Damping inter area oscillations of power systems by a fractional order PID controller. *IEEE International Conference on. Energy and Environment Technology*, 2, Pp. 103–106.

**Submitted:** 18/03/2017

**Revised :** 30/04/2017

**Accepted :** 15/09/2017

## تصميم مسيطر تناسبي تفاضلي تكاملي ذي رتبة كسرية لإخماد تذبذبات بينية واسعة منخفضة التردد باستخدام خوارزمية تطور التفاضلية

صالح بامسق\*، سريراما كومار ويوسف التركي

قسم الهندسة الكهربائية وهندسة الحاسبات، جامعة الملك عبد العزيز، جدة، المملكة العربية السعودية  
\* الشركة السعودية لتشغيل ومراقبة أنظمة الكهرباء، جدة، المملكة العربية السعودية

### الخلاصة

يمكن لنظام القياس واسع النطاق (WAMS) أن يعمل على توسيع وتحسين قدرة المسيطرات بفعالية لإخماد التذبذبات البينية منخفضة التردد في أنظمة القوى الكهربائية المترابطة. يقدم هذا البحث تطبيق مسيطر إخماد تناسبي تفاضلي تكاملي كسري المرتبة واسع النطاق (WA-FOPID) لتحسين إخماد النظام. تم اقتراح نهج التحليل الشكلي لتحديد أفضل موقع ل WA-FOPID والمزيج الأمثل لإشارات الإدخال. تم استخدام خوارزمية تطور التفاضلية المثلى لتحديد معلمات المسيطر الأمثل، وتمت صياغة دالة هدف غير خطية تستند إلى المجال الزمني لتقليل الأخطاء المرجحة زمنياً. تم تطبيق النهج المقترح بنجاح على نظام مكون من منطقتين وأربعة أجهزة، بالإضافة إلى نظام قوى طاقة متعدد المناطق. تشير المحاكاة غير الخطية للنطاق الزمني إلى أن WA-FOPID يستطيع إخماد التذبذبات البينية بشكل فعال وتحسين استقرار النظام، بغض النظر عن شدة أو اضطرابات الموقع.